The Submillimeter Spectral Energy Distributions of Herschel/SPIRE-Detected Galaxies

B. Schulz[1,2], C.P. Pearson[3,4], D.L. Clements5, A. Amblard[6], V. Arumugam[7], R. Auld[8], H. Aussel[9], T. Babbedge[5], A. Blain[1], J. Bock[1,10], A. Boselli[11], V. Buat[11], D. Burgarella[11], N. Castro-Rodriguez[12,13], A. Cava[12,13], P. Chanial[5], A. Conley[14], L. Conversi[15], A. Cooray[6,1], C.D. Dowell[1,10], E. Dwek[16], S. Eales[8], D. Elbaz[9], M. Fox[5], A. Franceschini[17], W. Gear[8], E. Giovannoli[11], J. Glenn[14], M. Griffin[8], M. Halpern[18], E. Hatziminaoglou[19], E. Ibar[20], K. Isaak[8], R.J. Ivison[20,7], G. Lagache[21], L. Levenson[1,10], N. Lu[1,2], S. Madden[9], B. Maffei[22], G. Mainetti[17], L. Marchetti[17], G. Marsden[18], A.M.J. Mortier[5], H.T. Nguyen[10,1], B. O'Halloran[5], S.J. Oliver[23], A. Omont[24], M.J. Page[25], P. Panuzzo[9], A. Papageorgiou[8], I. Perez-Fournon[12,13], M. Pohlen[8], N. Rangwala[14], J.I. Rawlings[25], G. Raymond[8], D. Rigopoulou[3,26], D. Rizzo[5], I.G. Roseboom[23], M. Rowan-Robinson[5], Douglas Scott[18], N. Seymour[25], D.L. Shupe[1,2], A.J. Smith[23], J.A. Stevens[27], M. Symeonidis[25], M. Trichas[5], K.E. Tugwell[25], M. Vaccari[17], E. Valiante[18], I. Valtchanov[15], L. Vigroux[24], L. Wang[23], R. Ward[23], G. Wright[20], C.K. Xu[1,2], and M. Zemcov[1,10]

1 California Institute of Technology, 2 IPAC/California Institute of Technology, 3 Rutherford Appleton Laboratory, 4 University of Lethbridge, 5 Imperial College London, 6 University of California, 7 University of Edinburgh, Royal Observatory, 8 Cardiff University, 9 Laboratoire AIM-Paris-Saclay, CEA/DSM/Irfu - CNRS - Universit'e Paris Diderot, 10 Jet Propulsion Laboratory, 11 Laboratoire d'Astrophysique de Marseille, OAMP, 12 Instituto de Astrof'isica de Canarias (IAC), 13 Universidad de La Laguna (ULL), 14 University of Colorado, Boulder, 15 Herschel Science Centre, European Space Astronomy Centre, 16 NASA Goddard Space Flight Center , 17 Universit' a di Padova, vicolo Osservatorio, 18 University of British Columbia, 19 ESO, Garching, 20 Royal Observatory, Edinburg, 21 Institut d'Astrophysique Spatiale (IAS) and CNRS, 22 The University of Manchester, 23 University of Sussex, 24 Institut d'Astrophysique de Paris, 25 University College London, 26 Oxford University, 27 University of Hertfordshire

We present colours of sources detected with the Herschel/SPIRE instrument in deep extragalactic surveys of the Lockman Hole, Spitzer-FLS, and GOODS-N fields in three photometric bands at 250, 350 and 500 μm. We compare these with expectations from the literature and discuss associated uncertainties and biases in the SPIRE data. We identify a 500 μm flux limited selection of sources from the HerMES point source catalogue that appears free from neighbouring/blended sources in all three SPIRE bands. We compare the colours with redshift tracks of various contemporary models. Based on these spectral templates we show that regions corresponding to specific population types and redshifts can be identified better in colour-flux space. The redshift tracks as well as the colour-flux plots imply a majority of detected objects with redshifts at 1<z<3.5, somewhat depending on the group of model SEDs used. We also find that a population of S250/S350 < 0.8 at fluxes above 50 mJy as observed by SPIRE is not well represented by contemporary models and could consist of a mix of cold and lensed galaxies.

Input Data and Processing

The HerMES key project is constructed in order to obtain a complete bolometric census of star formation in the Universe. It consists of 6 tiers of survey fields with increasing depth over smaller areas, covering most of the fields on the sky observed across the electromagnetic spectrum by state-of-the-art facilities plus individual selected clusters. A total of 4 HerMES fields were surveyed during Herschel's Science demonstration Phase (SDP) and we have used the deep observations in GOODS-N, Lockman-North, Spitzer-FLS, and Lockman-SWIRE for our analysis. The covered areas are 0.25, 0.34, 5.81 and 13.2 deg^2 respectively with relative depths of 1.0, 0.23, 0.05, 0.033 that were calculated as the fraction of the number of repeats and scan speed, normalised to the deepest field GOODS-N. More details of the observations are given by Oliver et al. (2010).

Data processing based on the standard SPIRE Scan Map Pipeline (Griffin et al. 2008) yielded maps in the three SPIRE bands, and source catalogues for each individual band were generated using the SUSSEXtractor software (Savage & Oliver 2007) within HIPE 3.0 (Ott et al. 2006). The three shallower maps were smoothed with point-source optimised filters while the deepest map was filtered with a delta function to find sources and separately with a 3 × 3 pixel PRF to extract the fluxes (Oliver et al. 2010). The FLS and Lockman-SWIRE fields were Wiener filtered to reduce effects by diffuse Cirrus. For the source extraction a Gaussian point source response function (PRF) was assumed, with FWHM of 18.2", 25.2" and 36.3" for the SPIRE 250, 350 & 500 μm bands, respectively. Details of the procedure are given by Oliver et al. (2010) and Smith et al. (2010). They attained formal 1-σ point source uncertainties of 5.7, 7.4 and 7.8 mJy for GOODS-N, 7.0, 8.5 and 8.8 mJy for Lockman-North, 9.0, 10.3 and 10.6 mJy for FLS, and 11.1, 16.9 and 15.1 mJy for Lockman-SWIRE, respectively. These numbers include a contribution from source confusion of approximately 5.6, 7.4, and 7.7 mJy for GOODS-N, 6.8, 8.3 and 8.5 mJy for Lockman-North, 8.4, 9.8, 9.7 mJy for FLS, and 8.5, 13.9, 10.2 for Lockman-SWIRE. For the two deepest fields Smith et al. (2010) attribute the differences to the results of Nguyen et al. (2010), and the differences between the fields mainly to the source extraction method used.

The catalogues contain additional parameters to allow for quality checking and source selection. These are: i) A formal error in the flux measurement, propagated through from the error maps created by the map-maker, representing a fair estimate of the instrumental noise. ii) A total error that is the quadratic co-addition of instrument noise and average estimated confusion noise over the map. iii) Two separate flux estimates for the same positions using two different halves of the data (half-maps), separated in time, allowing for the detection and exclusion of spurious sources, mostly due to high energy particle hits.

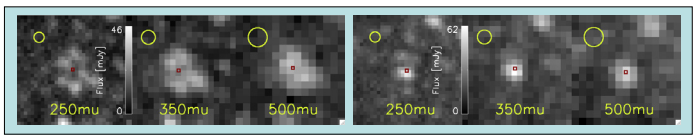

Fig. 1. Examples of single 500 μm source detections (top and bottom panel, right) with multiple counterparts at 350 μm and 250 μm (top panel, middle and left), and single 350 and 250 μm counterparts (bottom panel,middle and left). Note that the upper 500 μm source appears already double to the eye. The red marked source position in each image is the one determined by the algorithm at 500 μm. Each image measures 3' on each side. The yellow circles indicate the FWHM of the beams.

Catalogue Selection

The starting point for the cross-association process is this set of individual SPIRE band catalogues. For the current work the emphasis is on the creation of a robust, un-confused sample of sources that has the highest probability for its colours to originate from single unblended galaxies.We only consider the central regions of the maps, that have full homogeneous coverage by all scans. To protect against spurious sources, we compare fluxes separately derived from two independent half-maps. The ratio of the two flux estimates separates well into 3 distributions. Spurious sources are removed by excluding ratios above 5 and below 1/5.

For this work we have constructed a 500 μm band flux limited selection. It is justified in three ways: i) The stronger negative K-correction means selection in this band favours higher redshift galaxies; ii) This is a relatively new band as yet only explored by much shallower BLAST surveys (Devlin et al. 2009); iii) About 90% of 500 μm selected sources are also detected in the other SPIRE bands. We require a signal-tototal-noise (S/N) ratio of more than 3 in the 500 μm filter. The formal average flux uncertainties at 500 μm derived from the source extractor results are only 1.1, 2.1, 4.4, and 11.6 mJy. We consider these to be instrumental noise, based on their ratio, consistent with the 30, 7, 2, and 1 repetitions executed on the four fields, respectively, and the 1σ confusion noise at 500 μm of 6.8±0.4 reported by Nguyen et al. (2010). Thus the uncertainties are completely dominated by extragalactic confusion for the first two fields and increased for FLS and Lockman-SWIRE. We calculate the following effective 3σ average flux limits in our fields from 3 times the average total error of all sources with S/N< 4: 23.4, 26.4, 32.0, and 46.4 mJy for GOODS-N, Lockman-North, FLS, and Lockman-SWIRE respectively. The selection leaves 48, 61, 608, and 824 sources at 500 μm in the 4 bands respectively. This conservative threshold also minimises the impact of flux boosting on the derived colours of the sources.

To further de-blend and cross-match, first, all 500 μm sources without another 500 μm source within an 18" radius are selected. This radius was chosen to be similar to the beam size at 500 μm. Then for these remaining sources, the same 18" radius is checked in the other two bands. Sources with more than one source in a different band are discarded immediately. In case only one source is found in the other band, it must be within a radius of 8" in order to be accepted as a cross identification, otherwise the source is considered blended and discarded. This radius was chosen to include 3-σ of the telescope pointing error and the estimated PRF fit error of 6" each. We end up with a list of potentially uncontaminated 500 μm sources that is then cross matched with the lists of the other two bands with a match radius of 8".

This sample is largely free from contamination and should have reliable fluxes originating from just one source, accurate at a 30 % level or better. The final matched source numbers for the four fields respectively are 21, 38, 242, and 244.

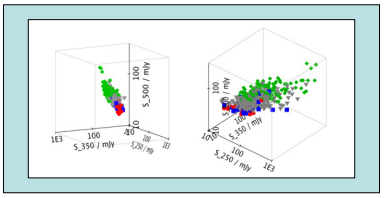

Fig. 2. The 3-dimensional flux parameter space for our unblended band-merged catalogues in the SPIRE 250, 350 & 500 μm bands. The sources in GOODS-N appear in red, Lockman-North in blue, FLS in grey, and Lockman-SWIRE in green. Both diagrams show the same 3D plot from two different aspect angles, the left one from within a plane fitted through the data, the other from a perpendicular direction.

Flux-Flux-Flux Degeneracy

The 3-dimensional SPIRE flux-flux-flux parameter space for our band merged catalogue. The fluxes are grouped around a relatively flat and thin surface in the 250 μm, 350 μm, 500 μm parameter space. The same even thinner surface is seen in similar plots of mock catalogue data. Thus, although we have flux data in three SPIRE bands, in principle only two parameters are needed to describe the information. This degeneracy follows from the fact that the spectral energy distributions (SEDs) in the submm, which SPIRE observes, are dominated by dust emission that have very similar shapes and result in fairly well defined flux ratios. Thus, the main parameters determining the three SPIRE fluxes, are rather wavelength of the emission peak and luminosity.

References

Dale, D. A., & Helou, G. 2002, ApJ, 576, 159
Devlin, M., Ade P.A.R., Aretxaga, I. et al., 2009, Nature, 458, 737
Griffin, M., Dowell, D.C., Lim, T., et al. 2008, Proc. SPIE, 7010, 70102,
Griffin, M. et al. 2010, A&A, , Herschel special issue.
Lagache, G., Dole, H., Puget, J.-L., 2003, MNRAS, 338, 555
Negrello, M., Perrotta, F., Gonzalez-Nuevo, J., Silva, L., de Zotti, G., Granato, G. L., Baccigalupi, C., & Danese, L. 2007, MNRAS, 377, 1557
Negrello, M., priv. comm.
Nguyen, H. T., Schulz, B., Levenson, L. et al., 2010, A&A, , Herschel special issue.
Oliver, S. et al., 2010, A&A, , Herschel special issue.
Ott, S., et al. 2006, Astronomical Data Analysis Software and Systems XV, 351, 516
Pilbratt, G. et al., 2010, A&A, Herschel special issue.
Pearson C., Jeong, W.S., Matsuura S. et al., 2007, Adv. Sp. Res., 40, 605
Rowan-Robinson M., et al., 2010, MNRAS, in prep.
Savage, R. S., & Oliver, S. 2007, ApJ, 661, 1339
Smith, A. et al., 2010, MNRAS, in prep.
Springel, V., et al. 2005, Nature, 435, 629
Valiante, E., Lutz, D., Sturm, E., Genzel, R., & Chapin, E. L. 2009, ApJ, 701, 1814
Xu, C., Lonsdale, C.J., Shupe, D.J. et al. 2001, Apj 562 179

Colour Colour Diagrams

In Figure 3 the S250/S350 - S350/S500 colour-colour diagrams for SPIRE sources in the SDP survey fields are shown with the colour tracks from the contemporary galaxy evolution models of Pearson et al. (2007), Dale & Helou (2002), Xu et al. (2001) & Lagache et al. (2003) over-plotted on individual panels. The redshift of the tracks is indicated in colour and ranges from 0 to 4. In general, all the models are consistent with the obtained SPIRE colours, except from individual subtleties of the models. All models agree: the colours imply that the SPIRE population is not local but rather the bulk lies at redshifts between 1 and 3.5. We note that the Xu et al. (2001) and Dale & Helou (2002)models tend to place the population at somewhat lower redshift than the other two. This implies that the Pearson et al. (2007) and Lagache et al. (2003) model SEDs contain generally warmer dust, which is confirmed by plots of the emission maxima of the SEDs.

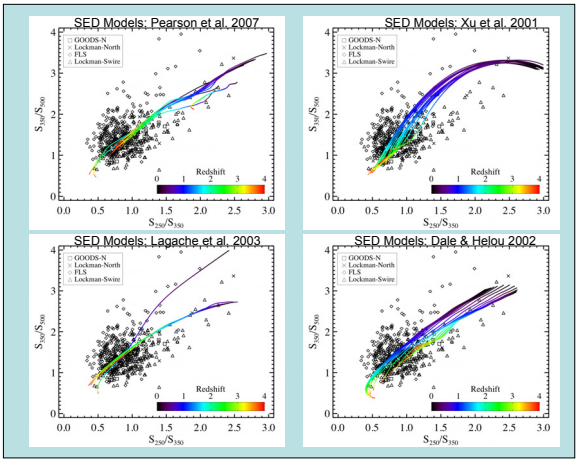

Fig. 3. S350/S500 - S250/S350 colour-colour plots for the SPIRE sources. Over plotted are the colour tracks from the galaxy evolution models of top-left Pearson et al. (2007), top-right Xu et al. (2001), bottom-left Lagache et al. (2003), and bottom-right Dale & Helou (2002). The redshift in the tracks is colour coded and runs from 0 to 4. The black symbols represent all unblended SPIRE sources according to the legend.

Colour Flux Diagram

To overcome the apparent degeneracy in the SPIRE colours (Figure 2), we plot colour-flux distributions. In Figure 4 we show the S250/S350 colour versus 500 μm flux density distributions for the SPIRE sources. A few sources at S500>100 mJy are not shown to improve visibility. The symbols indicate the different fields according to the legend in the upper left corner. The four crosses on the left are in the same vertical order as the symbols in the legend and represent the averaged uncertainties in the four fields. Different tickmarks show instrumental and total components. The five vertical lines indicate from left to right, three times the confusion noise limit from Nguyen et al. (2010), and the effective flux limits of GOODS-N, Lockman-North, FLS, and Lockman-SWIRE respectively. In both panels of Figure 4 the observed data are compared to mock catalogues of 1 deg^2 on the sky by Pearson et al. (2007) (left) and Xu et al. (2001) (right) that were cut below three times the confusion noise limit at 500 μm. The most notable difference is the larger spread of the Xu et al. (2001) colours as already apparent in Figure 3, due to a larger number and diversity of SED models. In both models the bulk of objects are Starburst galaxies, LIRGs and ULIRGs, that are grouped around a colour of S250/S350 ≈1.1. The high-redshift sources populate a specific area of the colour plane in both models, although the redshift distributions are different. In the Pearson et al. (2007) model the highest redshift objects, z>3 occupy the parameter space corresponding to S250/S350 colours <1.0 with S500 <40mJy, while the Xu et al. (2001) model locates the z>3 region rather at S250/S350 <0.8 and the same flux cutoff, but with fewer objects and mixed with many low redshift SEDs. Similar cuts can be made for z>2 sources. Lower redshift sources may also be excluded by virtue of their higher S250/S350 colours.

The SPIRE data generally overlap fine at S500<60 mJy, except for colours of S250/S350 < 0.8. Especially the Pearson et al. (2007) model shows no objects below this limit, while the same region is sparsely populated by the Xu et al. (2001) model SEDs. Looking at the model types, it turns out that those are mainly AGN, which are missing entirely in the Pearson et al. (2007) SED catalogue. Neither model covers sufficiently the increasingly redder colours in this region that SPIRE observes towards 500 μm fluxes above 50 mJy. A comparison with another mock catalogue by Valiante et al. (2009) shows the same lack of red sources.

A considerable fraction of submm bright sources are expected to be lensed by foreground galaxies (Negrello et al. 2007). Since lensing magnification is wavelength independent, such lensed sources appear in their intrinsic positions in the colour-colour diagram, but their locations in the colour-flux plane would be offset to brighter fluxes (towards the right side of Fig. 4 along the xaxis), while keeping colours the same. Using the models of Negrello et al. (2007) and Negrello priv. comm. (2010) we estimate that of all objects with fluxes S500 > 100 mJy and redshift 2<z<3, almost all are lensed. For our 19.6 deg^2 total sky area, that would be ≈2-3 out of the 24 bright 500 μm sources we have identified.

For now we conclude that we see a population of red bright objects that may consist mostly of colder SEDs but with a fraction of distant lensed ones. Inclusion of other wavelengths as shown by Rowan-Robinson et al. (2010) will be needed for further interpretation.

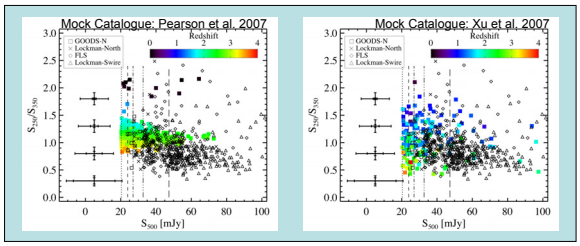

Fig. 4. Measured S250/S350 colour 500 μm flux distributions for the SPIRE sources (black symbols) in comparison with mock catalogues of Pearson et al. (2007) to the left and Xu et al. (2001) on the right. The large error crosses on the left represent average 1-σ total uncertainties dominated by extragalactic confusion and the smaller tick marks show instrumental noise only, which is negligible for GOODS-N and Lockman-N.

Acknowledgements

SPIRE has been developed by a consortium of institutes led by Cardiff Univ. (UK) and including Univ. Lethbridge (Canada); NAOC (China); CEA, LAM(France); IFSI, Univ. Padua (Italy); IAC (Spain); Stockholm Observatory (Sweden); Imperial College London, RAL, UCL-MSSL, UKATC, Univ. Sussex (UK); and Caltech, JPL, NHSC, Univ. Colorado (USA). This development has been supported by national funding agencies: CSA (Canada); NAOC (China); CEA, CNES, CNRS (France); ASI (Italy); MCINN (Spain); SNSB (Sweden); STFC (UK); and NASA (USA). Support for this work was provided by NASA through an award issued by JPL, Caltech. Data presented in this paper were analyzed using The Herschel Interactive Processing Environment (HIPE), a joint development by the Herschel Science Ground Segment Consortium, consisting of ESA, the NASA Herschel Science Center, and the HIFI, PACS and SPIRE consortia. The data presented in this paper will be released through the Herschel Database in Marseille HeDaM[2]. This work made substantial use of TOPCAT written by Mark Taylor[3]. We thank Mattia Negrello for predictions of lensed counts. Many thanks also to George Helou and an anonymous referee for helpful comments.
[2] hedam.oamp.fr/HerMES
[3] www.starlink.ac.uk/topcat